iScience

CellPress
OPEN ACCESS

Perspective

Plasmonic metal nanostructures: concepts, challenges and opportunities in photo-mediated chemical transformations

Weihui Ou,[1,2,5,6] Binbin Zhou,[1,2,5,6] Junda Shen,[2,3,4] Chenghao Zhao,[2,3,4] Yang Yang Li,[1,2,3,4,*] and Jian Lu[1,2,4,5,*]

SUMMARY

Plasmonic metal nanostructures (PMNs) are characterized by the plasmon oscillation of conduction band electron in response to external radiation, enabling strong light absorption and scattering capacities and near-field amplification. Owing to these enhanced light-matter interactions, PMNs have garnered extensive research interest in the past decades. Notably, a growingly large number of reports show that the energetics and kinetics of chemical transformations on PMNs can be modified upon photoexcitation of their plasmons, giving rise to a new paradigm of manipulating the reaction rate and selectivity of chemical reactions. On the other hand, there is urgent need to achieve clear understanding of the mechanism underlying the photo-mediated chemical transformations on PMNs for unleashing their full potential in converting solar energy to chemicals. In this perspective, we review current fundamental concepts of photo-mediated chemical transformations executed at PMNs. Three pivotal mechanistic questions, i.e., thermal and nonthermal effects, direct and indirect charge transfer processes, and the specific impacts of plasmon-induced potentials, are explored based on recent studies. We highlight the critical aspects in which major advancements should be made to facilitate the rational design and optimization of photo-mediated chemical transformations on PMNs in the future.

INTRODUCTION

Plasmonic metal nanostructures (PMNs) have garnered broad research interests owing to their strong interactions with incident light through localized surface plasmons (LSPs) that are the collective oscillation of free electrons under light excitation (Figure 1A). When the frequency of electron oscillation matches that of the incident light, localized surface plasmon resonance (LSPR) is established. Under the resonant conditions, PMNs display substantially larger optical extinction (absorption and scattering) cross-sections than their physical ones (Ming et al., 2012), along with remarkably intense local electric fields ($|E|^2$, compared with the incident field, Figures 1B and 1C) (Jiang et al., 2014). Following the excitation (Figure 1D), LSPs are relaxed by either re-emitting photons to free space (radiative decay) or yielding energetic charge carriers and heating up the crystal lattice (nonradiative decays) (Linic et al., 2015). By virtue of these unique optical properties, PMNs have been used in a wide range of applications, such as field-enhanced spectroscopy (Willets and Van Duyne, 2007), photodetection (Knight et al., 2011), photovoltaics (Atwater and Polman, 2010), imaging (Boyer et al., 2002), sensing (Liu et al., 2011), photothermal therapy (Ding et al., 2014), and so on.

In recent years, plasmon excitation of PMNs has been proved to be able to modify energetics and kinetics of chemical transformations, leading to more desirable reaction rate and/or product distribution at milder conditions than conventional thermal catalysis (Linic et al., 2011, 2015; Brongersma et al., 2015; Zhan et al., 2018; Kale et al., 2013; Corson et al., 2020). This burgeoning research field is commonly termed plasmon-mediated chemical reactions (PMCRs). PMCRs not only open up a new avenue to manipulate the reaction outcomes, which is otherwise difficult/unfeasible in dark conditions but also provide an efficient means for harvesting and converting solar energy through funneling the light energy into chemical bonds (Linic et al., 2015; Brongersma et al., 2015; Li et al., 2020a). To optimize the performance of PMCRs, their underlying mechanisms must be fully understood, which is under intensive scientific studies.

[1]Centre for Advanced Structural Materials, City University of Hong Kong Shenzhen Research Institute, Greater Bay Joint Division, Shenyang National Laboratory for Materials Science, Shenzhen 518057, China

[2]Hong Kong Branch of National Precious Metals Material Engineering Research Center, City University of Hong Kong, Hong Kong, China

[3]Center of Super-Diamond and Advanced Films (COSDAF), City University of Hong Kong, Hong Kong, China

[4]Department of Materials Science and Engineering, City University of Hong Kong, Hong Kong, China

[5]Department of Mechanical Engineering, City University of Hong Kong, Hong Kong, China

[6]These authors contributed equally

*Correspondence: yangli@cityu.edu.hk (Y.Y.L.), jianlu@cityu.edu.hk (J.L.)

https://doi.org/10.1016/j.isci.2020.101982

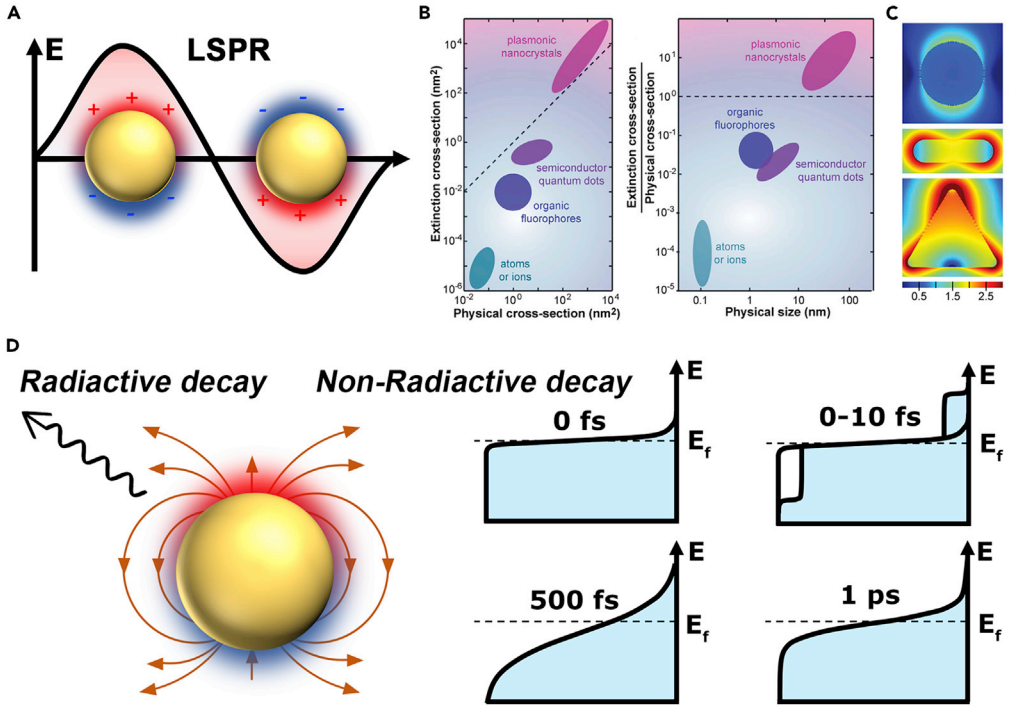

Figure 1. LSPR excitation and decay in PMNs, as well as their optical features

(A) Schematic illustration of collective oscillation of conduction-band electrons in PMNs.

(B) The extinction cross section versus the physical cross section of various nanoscale optical species (Ming et al., 2012).

(C) Logarithmic-scale electric field intensity amplification contours of differently shaped Au nanocrystals (Jiang et al., 2014).

(D) Radiative and nonradiative decay processes of LSPs in PMNs (Linic et al., 2015).

PMCRs are essentially heterogeneous catalytic processes involving multiple complicated interactions of three bodies: photons, PMNs, and reaction molecules. It is generally regarded that PMNs concentrate the energy of incoming photons in small volumes through their plasmonic oscillation of conduction electrons. Photothermal effects and energetic charge carriers from nonradiative plasmon decay are accounted for the observed desirable reaction results at illuminated PMNs. However, the individual contributions of photothermal effects and energetic charge carriers in PMCRs are still under vigorous debate (Zhou et al., 2018, 2019; Sivan et al., 2019a, 2020; Baffou et al., 2020; Dubi et al., 2020; Jain et al., 2020; Sivan et al., 2020). In addition, the specific mechanism by which energetic charge carriers interact with molecules that undergo chemical reactions needs to be further elucidated (Kale et al., 2013; Brongersma et al., 2015; Mubeen et al., 2013). Apart from the photothermal effects and energetic charge carriers, plasmon-induced potential was proposed to be responsible for the enhancement of reaction kinetics at illuminated PMNs in newly published studies (Wilson et al., 2019; Wang et al., 2020; Wilson and Jain, 2020). Herein, we give a brief introduction of pioneering and representative works about PMCRs and focus on three major aspects of the mechanism explanation, i.e., thermal and nonthermal effects, direct and indirect charge transfer, and plasmon-induced potentials. Critical viewpoints and perspectives on these issues are provided, in the hope of shedding some light on the mechanistic understanding and their industrial promises of PMCRs.

PLASMON-MEDIATED CHEMICAL REACTIONS

PMCRs feature a distinct reaction rate and/or product distribution at a milder reaction condition at the illuminated PMNs than the conventional thermal reactions. In 2013, Mukherjee et al. demonstrated the enhancement of dissociation rate of H_2 at Au nanoparticles (NPs) supported on the TiO_2 matrix under illumination (Mukherjee et al., 2013). By detecting the formation of HD molecules from the dissociations of H_2 and D_2, an almost 6-fold increase was identified (Figure 2A), which can be further improved by replacing TiO_2 with SiO_2 (Mukherjee et al., 2014). Illuminated nanostructured Ag was observed to accelerate catalytic oxidation reactions, such as ethylene epoxidation, CO oxidation, and NH_3 oxidation (Christopher et al.,

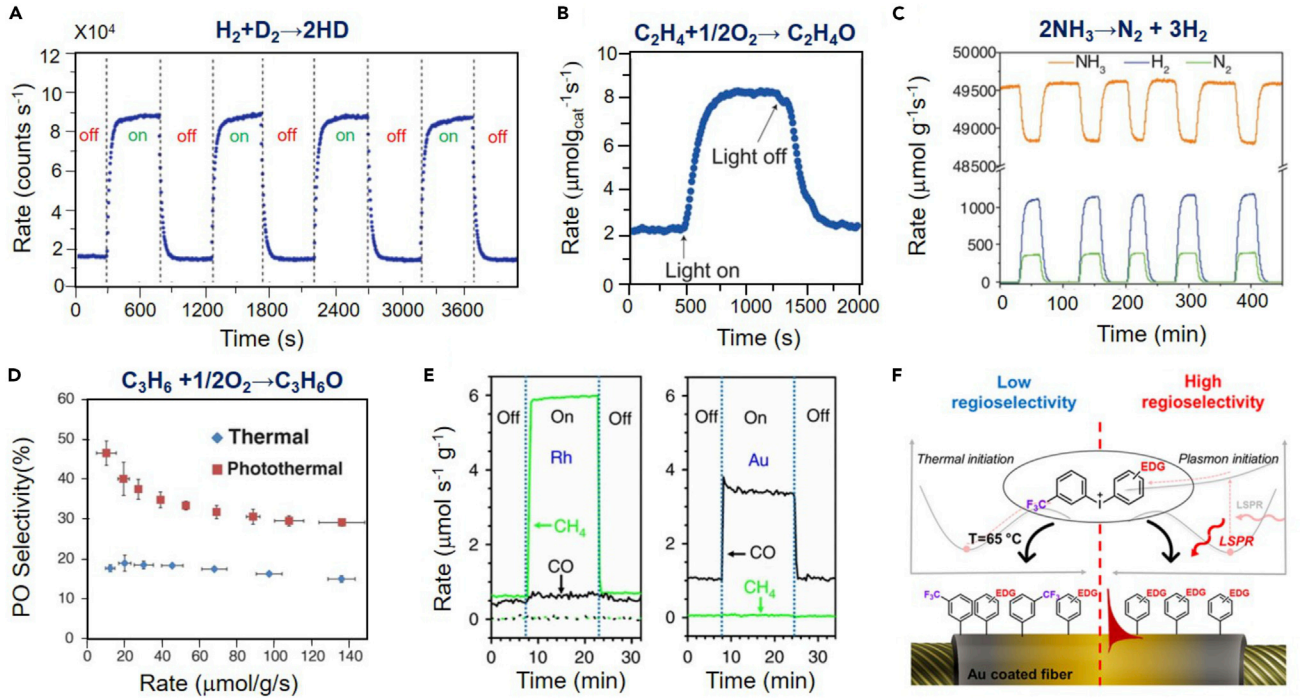

Figure 2. Photo-mediated chemical transformations on PMNs

(A) Real-time dissociation rate of H_2/D_2 on Au/TiO_2 photocatalyst with laser (2.41 W/cm^2) intermittently switched on/off (Mukherjee et al., 2013).

(B) The rate of ethylene epoxidation on plasmonic Ag with/without 250 mW/cm^2 visible light illumination (Christopher et al., 2011).

(C) Real-time rate of NH_3 decomposition on plasmonic antenna-reactor photocatalyst consisting of a Cu NP antenna and Ru reactor sites with 9.6 W/cm^2 white light switched on/off (Zhou et al., 2018).

(D) Selectivity to propylene epoxidation (PO) as a function of the reaction rate on Cu NPs with illumination by visible light at an intensity of 550 mW/cm^2 and in dark conditions (Marimuthu et al., 2013).

(E) Production rates of CH_4 and CO on Rh/Al_2O_3 (left) and Au/Al_2O_3 (right) with UV illumination at an intensity of 3W/cm^2 on/off (Zhang et al., 2017).

(F) The regioselective cleavage of unsymmetric iodonium salts on plasmonic Au (Miliutina et al., 2020).

2011, 2012). The steady-state reaction rate of ethylene epoxidation was increased about 4-fold with visible illumination at 250 mW/cm^2 compared with that of the thermal process (Figure 2B). A recent publication revealed that excited plasmon remarkably facilitated ammonia decomposition at plasmonic antenna-reactor photocatalyst that consisted of a Cu antenna and Ru reactor sites (Figure 2C) (Zhou et al., 2018).

In addition to achieving a desirable reaction rate, excited LSPs are able to manipulate product selectivity. The steady-state selectivity in propylene epoxidation at the surface of Cu NPs was considerably increased upon photoexcitation of Cu LSPs (Figure 2D) (Marimuthu et al., 2013). Excited LSPs of Al were proved effective for selective carbon dioxide conversion to carbon monoxide in the reverse water-gas shift reaction (Figure 2E) (Robatjazi et al., 2017). Postnikov et al. even demonstrated the probability of manipulating regioselectivity in cleavage reaction of unsymmetric iodonium salts by Au LSPs, opening a novel avenue for the fine control of reactivity in organic chemistry (Figure 2F) (Miliutina et al., 2020). Some other promising applications were reviewed in several excellent articles (Linic et al., 2011, 2015; Kale et al., 2013; Brongersma et al., 2015; Li et al., 2020a; Zhang et al., 2018a).

Alongside a growingly large number of studies on modifying chemical transformations by LSPs of PMNs, there is an urgent need for an accurate and deep mechanistic understanding of the observed plasmonic enhancement in PMCRs. It has been demonstrated that the plasmonic enhancements of PMCRs are intimately related to the confined intense electromagnetic fields, energetic charge carriers, and photothermal effects in optically excited PMNs. For example, the intense electromagnetic fields at the surface of illuminated Au NPs facilitate the polymerization of SU-8 that is a triarylium-sulfonium salt-based photo-initiator (Ueno et al., 2008). The photothermal effects promote the decomposition of dicumyl peroxide to 2-phenyl-2-propanol and acetophenone on illuminated Au NPs (Fasciani et al., 2011). Energetic charge carriers

enhance carbon dioxide reduction, O_2 dissociation and oxidation reactions, H_2 dissociation and hydrogenation reactions, N_2 fixation and NH_3 decomposition, and CO_2 reduction and/or dissociation on PMNs (Li et al., 2020a). More encouragingly, some studies at single particle and single turnover event level provide invaluable insights into the fundamental processes of PMCRs, e.g., the rate-determining step and its activation energy, and the spatial distribution of reaction sites (Zhao and Chen, 2020; Tachikawa et al., 2013). By using single-molecule fluorescence, the plasmon enhanced-fluorogenic oxidation of Amplex Red by H_2O_2 on a single Au nanorod was investigated with sub-turnover resolution (Li et al., 2020b). The activation energies of intermediate generation, product generation, and product desorption were clearly differentiated, showing that the excited LSPs mainly accelerate the intermediate generation (rate-limiting step) by substantially lowering its activation energy. Dionne et al. demonstrated that LSPs drive reaction nucleation at specific sites closest to the electromagnetic hot spots in the dehydrogenation of Pd nanocubes adjacent to an Au nanodisc by employing a light-coupled environmental transmission electron microscopic and claimed that Au LSPs enhance direct absorption within the hybridized Pd–H molecular orbitals, improving reaction rate and site selectivity (Vadai et al., 2018). Cortes et al. ambiguously demonstrated the localization of reactive spots in PMCRs through single-antenna SERS (surface-enhanced Raman spectroscopy) detection of energetic electron reduction from 4-NTP to 4-ATP on Ag (Cortes et al., 2017). Although these achievements shed light on some important elemental processes of chemical transformation on PMNs, our mechanistic understanding of PMCRs is far from complete.

THERMAL AND NONTHERMAL CONTRIBUTIONS

One of the key questions is whether PMCRs are primarily driven by energetic charge carriers or photothermal heat. As demonstrated in Figure 1, LSPs set off a cascade of physical processes that are expected to mediate the chemical transformations at PMNs. Their contributions can be classified into two categories: nonthermal effects (charge carrier-driven reaction) and thermal effects (heat-driven reaction). In other words, should the observed improvement of PMCRs be mainly ascribed to nonthermal or thermal effects in essence, and how to quantify their individual contribution?

In the study on the dissociation reaction of H_2 at Au/TiO_2 (Mukherjee et al., 2013), the authors justified plasmon-induced H_2 photodissociation by the agreement between the wavelength dependence of reaction rate and the calculated absorption cross section and measured diffuse reflectance spectrum of Au/TiO_2 (Figures 3A and 3B). This is also the most common practice in most publications at present. When the system was heated up to the same temperature (measured by a thermocouple) under illumination, only a slight increase in reaction rate was observed, far smaller than that under illumination (Figure 3C). Based on this observation, they claimed that the enhancement of reaction rate under illumination was caused by energetic electrons from the decay of Au LSPs. They further proposed a mechanistic picture by combing the density functional theory (DFT) and embedded correlated wave function calculations. The energetic electrons are injected into the antibonding state of the H_2, creating a transient negative ion ($H_2^{\delta-}$) whereby its bond length was extended. Subsequently, $H_2^{\delta-}$ relaxes to the ground-state potential energy by transferring the electron back to Au and dissociates (Figure 3D).

The above-mentioned thermal control experiment actually has been popularly utilized to disentangle nonthermal effects from thermal effects in other PMCRs. In the study on photocatalytic ammonia decomposition at Cu-Ru surface alloy, Halas et al. quantified the contributions of energetic electrons in photocatalysis by subtracting thermal effects obtained by thermal control experiment (measured by thermal imaging camera) (Zhou et al., 2018). Moreover, they demonstrated that energetic electrons substantially reduced reaction energy barrier by fitting reaction rate as a function of temperature at various light wavelengths and intensity to Arrhenius equation (Figures 3E and 3F). The increase in reaction order upon illumination further suggested that energetic electrons decreased the surface coverage of adsorbed intermediate N, leading to a lower reaction energy barrier (Figure 3G). In the work of O_2 dissociation in ethylene epoxidation, Christopher et al. found that the kinetic isotope effect (KIE), the ratio of steady-state rate by exploring the O_2^{16} and O_2^{18} isotopes, was lager under illumination (from ~1.09 to ~1.49) than thermocatalysis (~1.09), providing another evidence for energetic electron-driven reaction (Figure 3H). They demonstrated that the rate of such an energetic electron-driven reaction rate exhibited super-linear dependence on illumination intensity, which was rooted in the multiple excitations of absorbates before overcoming the activation barrier at high light power (Figures 3I and 3J). Overall, these works argued that PMCRs were dominated by nonthermal effects in which the transfer of energetic charge carriers excited the entire adsorbate-PMN system, leading to enhanced reaction rates and/or product distributions.

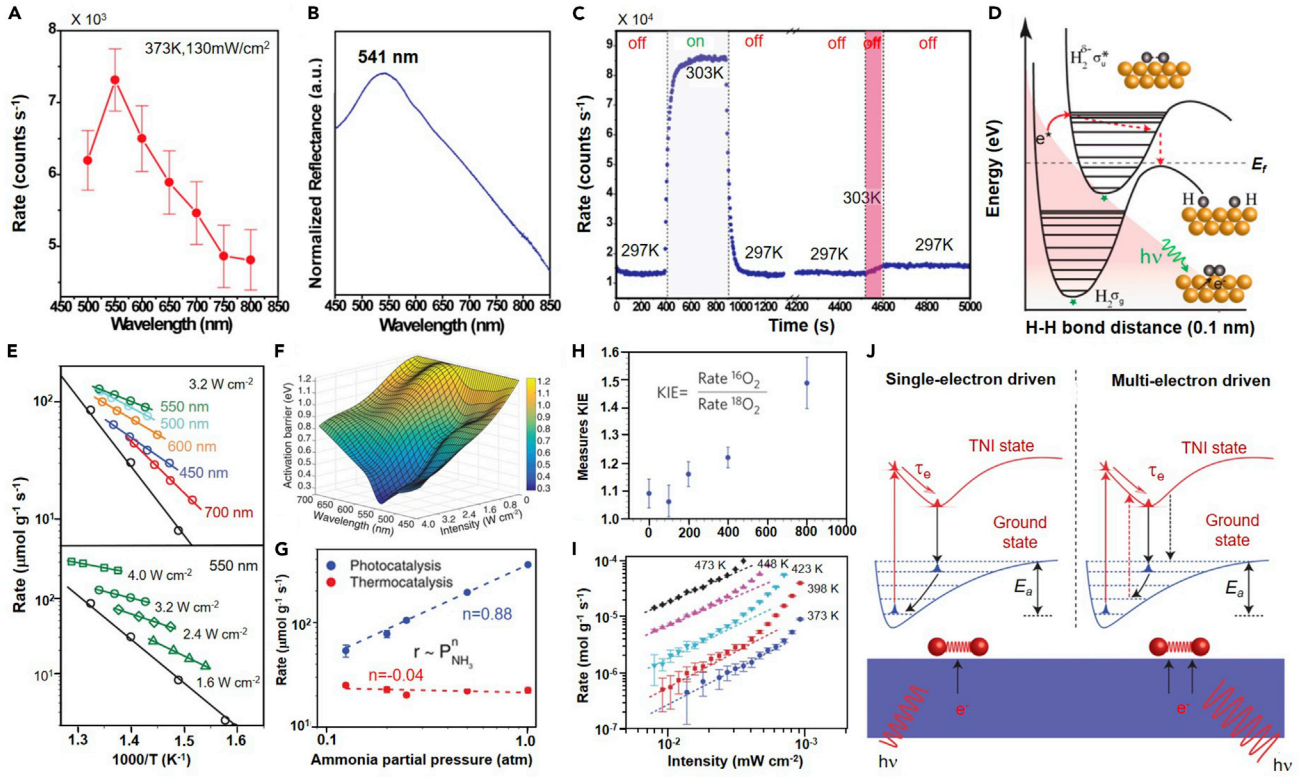

Figure 3. Nonthermal explanation for chemical transformations on PMNs

The wavelength dependence of reaction rate (A), the diffuse reflectance spectrum of powdered Au/TiO_2 photocatalyst (B), the comparison of reaction rate in photocatalytic experiment and thermal control experiment (C), and proposed mechanism (D) in the dissociation reaction of H_2/D_2 on Au/TiO_2 photocatalyst (Mukherjee et al., 2013). The reaction rate as a function of the reciprocal of measured temperature for (A) different wavelengths under constant intensity and various light intensities at 550 nm (E), 3D representation of activation barrier for different wavelengths and intensities (F), and the reaction order with respect to partial pressure of NH_3 in photocatalysis (G) in NH_3 decomposition on Cu-Ru plasmonic antenna-reactor photocatalyst (Zhou et al., 2018). The KIE (H) and reaction rate (I) as a function of light intensity, as well as the schematics of single electron-driven and multiple electron-driven mechanism (J) in O_2 dissociation process on plasmonic Ag (Christopher et al., 2012).

However, this popular explanation has been questioned recently (Sivan et al., 2019a, 2019b, 2020; Baffou et al., 2020; Dubi et al., 2020). Sivan et al. claimed that there existed a rather long series of experimental flaws in those articles, leading to the measured temperature being remarkably smaller than the actual one under illumination. As results, the thermal effects under illumination, which were mimicked from thermal control experiment, were severely underestimated or misinterpreted as nonthermal effects. Moreover, they proposed alternative interpretation for some key experimental observations based on Fermi golden rule and a purely thermal Arrhenius law with a fixed activation energy and intensity-dependent heating. They argued that thermal effects were responsible for the improved results of chemical transformations at illuminated PMNs. We hereafter outline their criticism about the experimental procedures and interpretation of the experimental results from several important articles in this field.

In the case of dissociation of H_2 at Au/TiO_2 (Mukherjee et al., 2013), the temperature was measured by a thermocouple placed a few millimeters away from the reactor chamber. Given the substantial temperature variation inside the chamber, the actual temperature of reaction sites under illumination is very likely larger than 30°C (Figure 3C), resulting in the underestimation of thermal effects. The invalidity of thermal control experiment therefore cannot support the interpretation of rate enhancement as nonthermal effects. Instead, Sivan et al. invoked Arrhenius law to explain the experimental results with assumption of the linear dependence of light intensity (I_{inc}) on the actual reactor temperature $T(I_{inc})$, namely, Equations 1 and 2:

$$T(I_{inc}) = T_{dark} + aI_{inc} = T_M + \tilde{a}I_{inc} \quad \text{(Equation 1)}$$

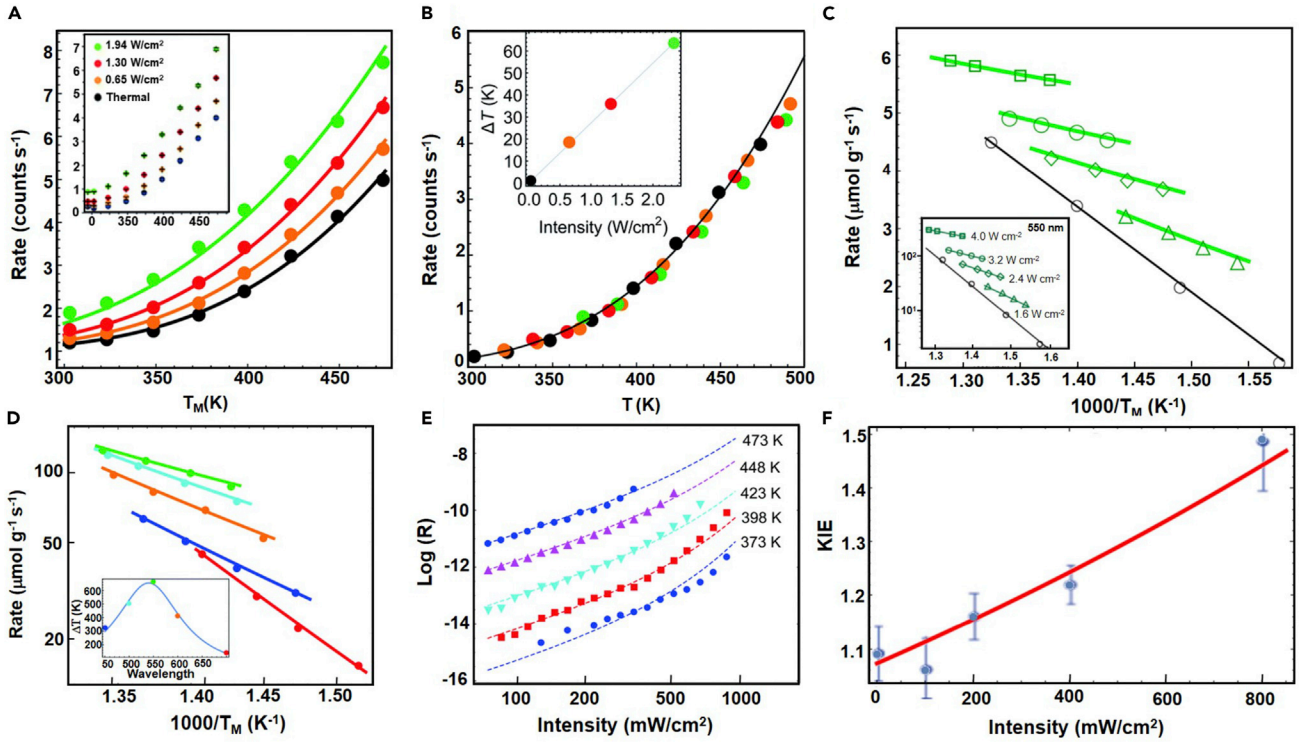

Figure 4. Thermal explanation for chemical transformations on PMNs

(A) Reaction rate as a function of the measured temperature in the plasmon-induced dissociation reaction of H_2/D_2 on Au/TiO_2 for different light intensities. The solid circles are experimental data, whereas the solid lines are the fitting results based on Equations 1 and 2 (Dubi et al., 2020).

(B) The temperature values (solid circles) calculated by shifting the measured temperature in (A) subject to Equation 1 (inset), with all data perfectly matching the fitting curves (solid line). Reproduction of the reaction rate as a function of inverse (average measured) temperature, based on Equations 1 and 2, for different light intensities (C) and wavelengths (D) in plasmon-enhanced NH_3 decomposition on Cu-Ru (Sivan et al., 2019a; Dubi et al., 2020). Reproduction of the superlinear dependence of reaction rate on light intensity (E) as well as KIE effects (F) in O_2 dissociation process on plasmonic Ag by using purely photothermal theory under plasmonic excitation (Dubi et al., 2020).

$$R = R_0 \exp\left(-\frac{\varepsilon_a}{k_B T(I_{inc})}\right) \qquad \text{(Equation 2)}$$

where T_{dark} and T_M denote the measured temperature of the reactor in the dark and under illumination, respectively. The terms, a and $\tilde{a}$ are photothermal conversion coefficients. k_B is the Boltzmann constant, ε_a is the reaction activation energy, and R_0 is a constant (Dubi et al., 2020). First, they extracted ε_a (~0.23 eV) by fitting Equation 2 to the experimental data in dark (Figures 4A and 4B). Then, with ε_a and 5.2-fold reaction enhancement known, T_{inc} was calculated as 362 K from Equations 1 and 2, 59 K larger than T_M (303 K). Together with the known incident laser intensity I_{inc} of 2.4 W/cm^2, $\tilde{a}$ was extracted as 27.2 K cm^2/W. At last, they successfully reproduced the experimental data by Equations 1 and 2 with no additional fitting parameters. A similar thermal explanation was suitable for H_2 dissociation at Au/SiO_2 under illumination (Dubi et al., 2020). As for ammonia decomposition at Cu-Ru, the authors tracked the reaction temperature using a thermal imaging camera, concluding that energetic electrons accelerated reaction by lowering the reaction activation barrier (Zhou et al., 2018). However, it was argued that the measured temperature was lower than the true temperature due to inappropriate settings of emissivity and improper focusing (Sivan et al., 2019a). In addition, thermal camera measured the average temperature throughout the sample due to limited spatial resolution, whereas catalytic rates reflected an exponential average of temperature. These discrepancies undermine the effectiveness of thermal control experiment, and thus possibly make the derived conclusion less convincing. Sivan et al., instead, reproduced the dependence of reaction rate on inverse measured temperature at various light wavelengths and intensity by employing Equations 1 and 2 and two sets of experimental data (Figures 4C and 4D), providing a purely thermal explanation for observed rate enhancement. Moreover, the purely thermal explanation was effective for the super-linear dependence of reaction rate on light intensity and the larger KIE, which were

previously assumed the important signatures of charge carrier-driven reaction (Figures 4E and 4F). In a word, they argued that there was nothing special in using PMNs for photocatalysis, and that thermal effects were dominantly responsible for the modified reaction outcomes.

Undoubtedly, the discussion over the thermal effects and nonthermal effects benefits future experimental design and result analysis in this rapidly growing field. To accurately evaluate thermal effects in PMCRs, the thermal control experiment should be carried out with extreme cautions. Notably, one has to acquire the temperature profile of illuminated PMNs as accurately as possible. To achieve that, some necessary measures should be taken, such as employing thin pellets or dilute PMNs as sample to minimize thermal inhomogeneity, choosing best emission values and focus distance for a thermal camera, and avoiding the impingement of light on thermocouple. Alongside, novel temperature-measuring techniques with nanoscale spatial and femtosecond timescale resolution needed to be developed due to the ultrafast dynamics and highly localized LSPs' induced heating (Baffou et al., 2010a, 2010b; Engelbrekt et al., 2020). Deckert et al. recently reported such an attempt in which the temperature of a single plasmonic hotspot was derived by the tip-enhanced Raman technique (Richard-Lacroix and Deckert, 2020). Cortes et al. developed a method to *in situ* characterize the photothermal effects of single NPs by exploiting anti-Stokes thermometry, which is label-free, applicable to any NPs with detectable anti-Stokes emission, and does not require any prior information about the NP or the surrounding media (Barella et al., 2020). In addition, the development of temperature calculation will also be of paramount importance for understanding the temperature evolution as well. For example, the temperature increment of randomly distributed ensembles of PMNs was predicted several orders of magnitude larger than that of single PMN due to photothermal collective effects (Richardson et al., 2009; Baffou et al., 2013, 2020; Un and Sivan, 2020; Maley et al., 2019). It is worth mentioning that single-particle techniques may be powerful tools to disentangle the role of energetic charges and thermal effects, thanks to their ultrahigh spatiotemporal definition (Zhou et al., 2012; Andoy et al., 2013). Chen et al. identified a huge heterogeneity of catalytic activity among the Au nanocrystals based on the wide distributions of activation energies across multiple individual nanocrystals (Chen et al., 2016). They further imaged the reaction hotspots on single plasmonic metals via correlated super-resolution and electron microscopy (Zou et al., 2018). By comparing the image of reaction hotspots to that of thermal hotspots (Baffou et al., 2010a, 2010b), the contribution of thermal effects in PMCRs may be extracted. Nevertheless, the researchers have to always keep in mind that thermal control experiment is not able to completely reproduce the photothermal effects in PMCRs. Multiple results obtained through varying experimental parameters, such as the illumination time, polarization, spot size wavelength, and intensity of light, should be accounted for separating the contributions of thermal and nonthermal effects (Baffou et al., 2020). Fortunately, we can roughly estimate the extent to which the measurement errors of temperature (ΔT) would impact the reaction rate by using Arrhenius law for most PMCRs. For instance, a ΔT of 50 K will result in about 46-fold changes of reaction rate with ε_a at 2.2 eV and the real temperature (T_r) of 550 K, which would be reduced for a higher T_r and smaller ε_a (Figures 5A and 5B). This suggests that quantification of the contribution of energetic electron based on thermal control experiment is more reliable for the PMCRs that possess small activation barrier and are executed at high temperature.

On the other hand, an alternative method to differentiate and rank thermal and nonthermal effects, which is not based on the thermal control experiment, should deserve much attention. For example, Ou et al. differentiated and quantified energetic charge carriers and photothermal effects by virtue of their highly different transport distances at plasmonic Ag nanostructures (Figures 5C and 5D) (Ou et al., 2020). As can be seen from Figure 5C, the photocurrent of plasmonic Ag electrode consists of a rapid (green line) and a subsequent slow (red) response current. By contrast, only a slow response current was observed when the light was impinged at the part of plasmonic Ag electrode above the liquid level. Because the hot electrons are highly localized (Brown et al., 2016), whereas heat can transfer along the electrode for a longer distance to reach reaction sites in the electrolyte, the rapid and slow response current (green line) can be ascribed to nonthermal effects and thermal effects in plasmon-mediated electrochemical reactions at Ag electrode, respectively. Although this method excluded the errors brought by the inaccuracy of temperature measurement in thermal control experiment, the specific spatiotemporal dynamics of hot electron and heat, which are intimately related to the response currents in PMCRs, remains elusive. Recently, some elegant attempts to shed light on these fundament processes have been reported. Block et al. revealed that hot-electron diffusion in thin gold films features a rapid diffusion during the first a few ps and a subsequent 100-fold slower diffusion at longer times by using ultrafast thermomodulation microscopy (Block et al., 2019). It was demonstrated that heat diffusion can be faster than electron-phonon

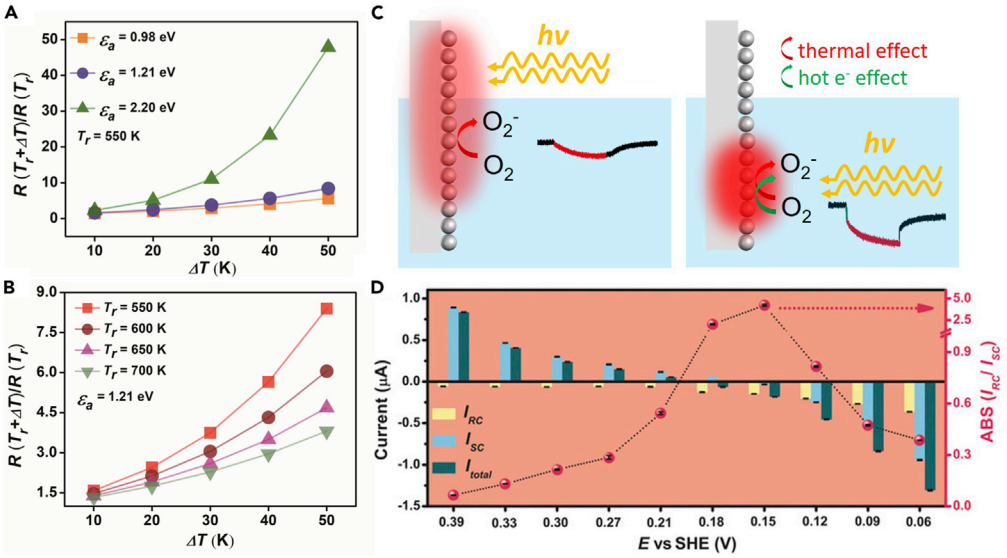

Figure 5. The method that is not based on temperature measurement to disentangle thermal from nonthermal contributions

(A and B) The variation of reaction rate as a function of the measurement errors of temperature, ΔT, at various activation energy barriers, ε_a, (A) and real temperature, T_r (B).

(C) Schematic illustration of disentangling nonthermal and thermal effects in electrochemical reaction proceeding at nanostructured Ag electrode by illuminating at different locations (Ou et al., 2020).

(D) Rapid-response current (I_{RC}, nonthermal effects), slow-response current (I_{SC}, thermal effects), total photocurrent (I_{total}, total effects), and the ratio of I_{RC} to I_{SC} at different electrode voltages with laser switched on-off (Ou et al., 2020).

energy transfer rate (Sivan and Spector, 2020). Similar strategies that bypassed the temperature measurement were also explored to quantify these two effects in electrochemistry at plasmonic Au electrode (Zhan et al., 2019; Rodio et al., 2020; Yu et al., 2018a, 2018b; Schorr et al., 2020). Also, the deeper mechanistic study on both thermal and nonthermal effects has to receive continuous efforts. For instance, Caleb and Kwillets et al. demonstrated that thermal effects are related to the enhanced local mass transport and the shifts in equilibrium redox potentials (Maley et al., 2019; Yu et al., 2018a, 2018b; Schorr et al., 2020). Apart from energetic charge carriers, plasmon-induced potential was also found to contribute to nonthermal effects (Ou et al., 2020). It was even proposed that heat and energetic charge carriers worked synergistically in certain reaction (Zhang et al., 2018b). To sum up, a clear separation and quantifying of thermal effects and nonthermal effects in PMCRs remains a grand challenge yet.

DIRECT AND INDIRECT CHARGE TRANSFER

In the charge carrier-driven reaction, it was conceptually established that energetic charge carriers generated from nonradiative LSP decay would be transferred to the unpopulated electronic states of adsorbates at PMNs. To date, there exists two ways by which the energetic charge carriers were attached to the adsorbates on the surface of optically excited PMNs (Figure 6A).

One is indirect charge transfer mechanism. In this case, LSPs nonradiatively decay into single electron/hole pair excitations via Landau damping within ~10 fs after excitation (Figure 1D) (Li et al., 2013; Linic et al., 2015). These nonthermal energetic charge carriers will redistribute their energy among electrons with lower energy via electron-electron scattering, leading to a new Fermi-Dirac-like distribution at elevated electron temperature around several hundreds of femtoseconds (Sun et al., 1994). All carriers above or below the Fermi level are chemically active, favoring the specific reactions after they were attached to the acceptor orbitals of absorbates. For example, Moskovits et al. reported an autonomous solar water-splitting device based on Au nanorod arrays coated with Pt and Co as cocatalysts and demonstrated that the hydrogen and oxygen evolution were, respectively, driven by energetic electrons and holes from the nonradiative decay of Au LSPs (Mubeen et al., 2013). Cortes et al. studied the electro-oxidation and electro-reduction of polyaniline on a single Au NP by combining dark-field microscopy and photoelectrochemistry, unveiling that the energetic holes on the Au NPs are responsible for plasmonic catalysis and that the energy of holes

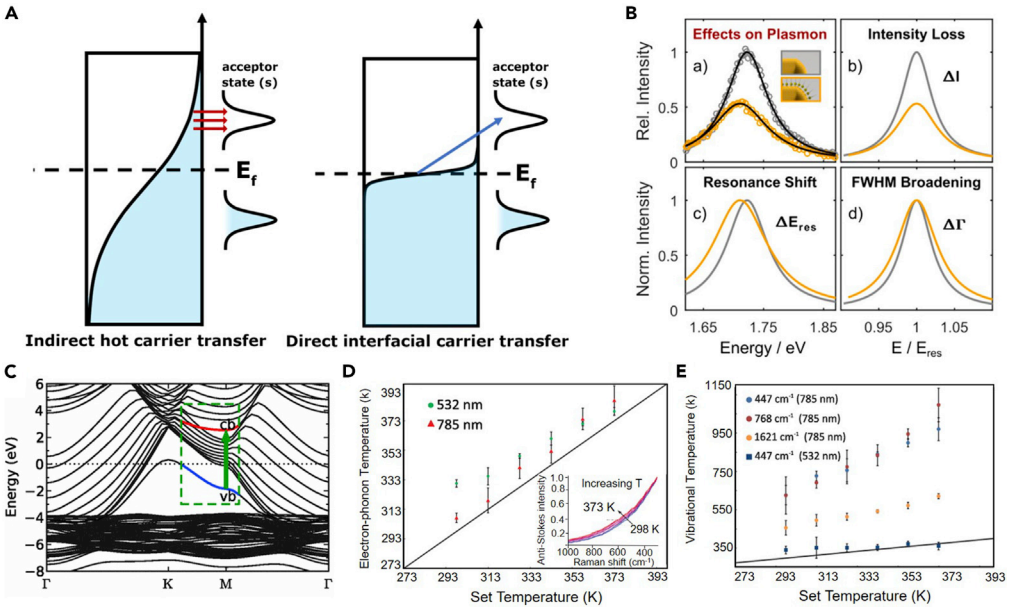

Figure 6. Mechanisms of indirect and direct charge transfer in PMCRs

(A) Proposed indirect and direct charge transfer progresses (Kale et al., 2013).

(B) Changes in spectrum, the scattering intensity ΔI, the resonance energy ΔE_{res}, and the line width $\Delta \Gamma$ of an Au nanorod before (gray) and after (yellow) functionalization with dodecanethiol (Foerster et al., 2017).

(C) Band structure of the Ag (111) surface with an adsorbed monolayer of H_2, and direct charge transfer from valence band (blue) to conduction band (red) (Yan et al., 2011). Temperature variations of (D) Ag NPs and (E) vibrational modes of methylene blue adsorbed on Ag NPs under plasmonic excitation (Boerigter et al., 2016).

is highly light wavelength dependent (Simoncelli et al., 2019). In the study on plasmon-mediated cleavage of thiol molecules on the surfaces of Au NPs by single-molecule super-resolution fluorescence microscopy, they uncovered that energetic electrons are responsible for triggering the Au-S bond cleavage, and mapped -the energetic electron active sites that are highly localized and can be manipulated by varying the wavelength and polarization of light excitation (Simoncelli et al., 2018). To date, the indirect charge transfer mechanism is most frequently invoked to explain PMCRs.

The other is direct charge transfer mechanism. In this scenario, the interaction of LSPs with adsorbates directly injects energetic charge carriers to unpopulated adsorbate states at the instant of LSPs' dephasing, rather than some time after dephasing (Kale et al., 2013; Kumar et al., 2019; Rao et al., 2019). This direct charge carrier transfer progress is also termed chemical interface damping (CID). Electromagnetic simulation can provide rich information regarding the spatial distribution of the near field around PMNs, which is beneficial for fundamental understanding of the generation and transport of energetic charges in the indirect charge transfer mechanism. However, current electromagnetic modeling is much less effective in CID. The chemical interface of PMNs and absorbates would modify the surface electronic structure near Fermi level of PMNs, changing their plasmonic properties, e.g., broadening plasmon line width and shifting resonant energy (Figure 6B) (Foerster et al., 2017; Zijlstra et al., 2012; Therrien et al., 2019). This process is concurrent with three-body interaction, i.e., PMN, absorbate, and photon, whereas the current electromagnetic modeling of plasmons scarcely incorporates the complex electronic and structural interaction between PMN and absorbate. Electron transfer proceeded via this mechanism both in the H-Ag complex (Figure 6C) (Yan et al., 2011) and at an Ag-CO interface at plasmonic excitation (Kumar et al., 2019). Linic et al. found that the temperature of methylene blue vibrational modes is exceptionally larger than the electron-phonon temperature of the supporting Ag nanocubes under 785 nm illumination (Figures 6D and 6E), which is impossible in indirect charge transfer mechanism, thus providing solid experimental evidence for this direct charge transfer mechanism (Boerigter et al., 2016).

Indirect and direct charge transfer mechanisms affect the outcomes of chemical reactions differently. In terms of indirect charge transfer process, a lot of energetic charge carriers are relaxed back to the Fermi

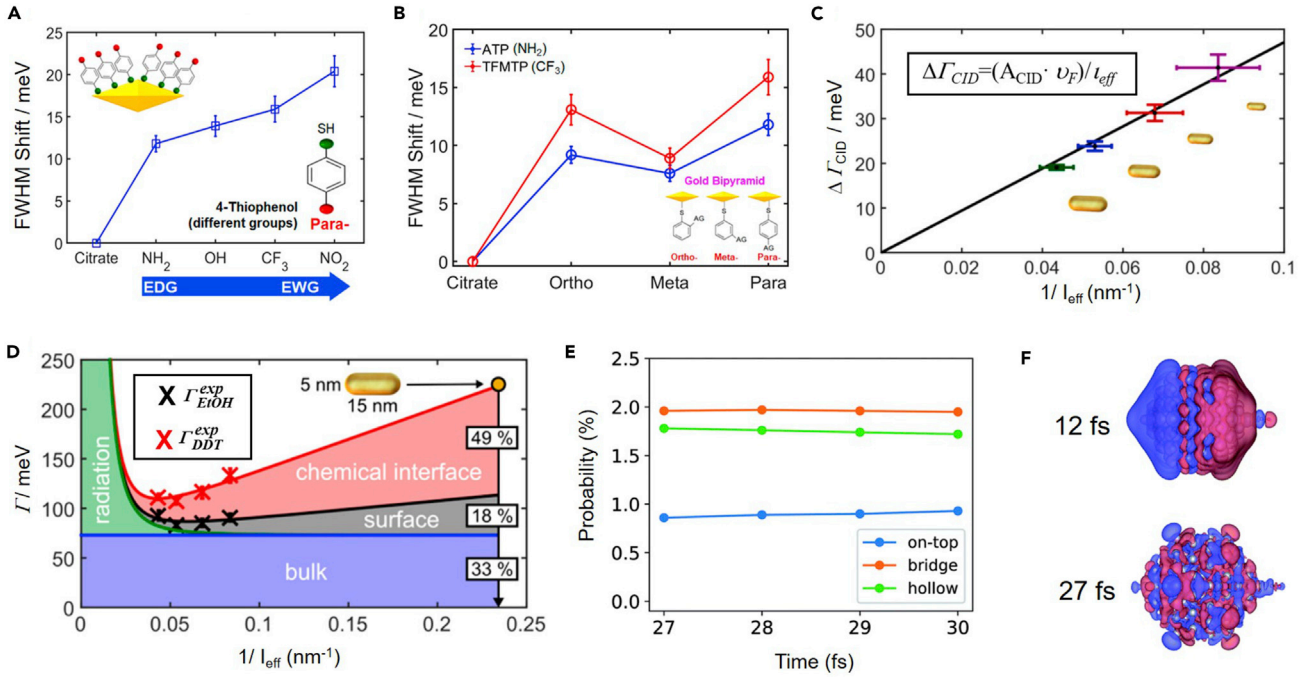

Figure 7. Mechanistic study on direct charge transfer in PMCRs

(A and B) The shift in the LSPs' resonant peak line width of Au bipyramid nanocrystals with (A) increasing electronic effects of the group (EDG to strong EWG) and (B) change in its substitutional position in thiophenol (Lee et al., 2019).

(C) Average chemical interface damping ($\Delta\Gamma_{CID}$) of single Au nanorods functionalized with dodecanethiol as a function of the effective electron path length ($1/l_{eff}$) (Foerster et al., 2017).

(D) Size ($1/l_{eff}$)-dependent contributions of the four competing damping channels: radiation damping, bulk damping, electron surface scattering, and CID (Foerster et al., 2017).

(E) Probability of the direct hot electron transfer from Ag to the adsorbate CO at different the binding sites (Kumar et al., 2019).

(F) Charge densities of Ag NP at 12 and 27 fs in response to the 10-fs laser pulse. Red and blue colors denote positive and negative charges, respectively (Kumar et al., 2019).

level before they are injected to reactants to trigger chemical transformations. As a result, the conversion efficiency of photon energy into chemical energy is very low. In addition, the high abundance of low-energy electrons near the Fermi level in illuminated PMNs would comprise the product selectivity because only absorbates with unoccupied orbitals close to the Fermi level would be activated (Linic et al., 2015; Reddy et al., 2020). In the case of direct charge transfer process, energetic charge carriers are coherently injected into the unoccupied states of absorbates without those carrier relaxations, thus providing a much more efficient channel to reserve the solar energy in chemical bond. More importantly, direct charge transfer process is the attachment of charge carrier to a specific orbital within the reactants, resulting in the preferential activation of a particular chemical bond. This process enables a great potential in tuning of the product selectivity by engineering the chemical interface of PMNs and reactants as well as excited light in PMCRs.

To take full advantages of the potentials in direct charge transfer progress, much more efforts need to be made in the following fields. First, it is of utmost importance to fully uncover how the electronic and structural properties of absorbate molecules at the surface of PMNs affect the direct charge transfer process. For example, Lee et al. demonstrated that direct charge transfer in Au-thiophenol interface can be controlled by the electron-withdrawing/-donating feature and location of functional groups at thiophenol molecules (Lee et al., 2019). It was found that electron-withdrawing groups (EWG) would induce larger homogeneous LSPs' peak widths than electron-donating groups (EDG), which indicates a higher electron injection rate from Au to thiophenol molecules (Figure 7A). They also showed that the *meta* position of EDG exhibited the lowest electron injection rate with respect to the *ortho* and *para* positions (Figure 7B). Second, a better understanding of the dependence of direct charge transfer efficiency on the morphology, dimension, and nature of PMNs is highly desirable. Au bipyramids with sharp tips were observed to show a higher electron injection rate than Au nanorods by reducing the effective transport distance of

electrons (Lee et al., 2019). Slink et al. unraveled that the energy transfer associated with direct charge transfer in Au nanorod-dodecanethiol interface is inversely proportional to the average distance of electrons to the surface and thus increases rapidly with decreasing size of the gold nanorods (Figure 7C) (Foerster et al., 2017). Third, we should develop reliable methods to quantify the contributions of direct and indirect charge transfer to the enhancement of reaction rate because these two effects may occur simultaneously in most PMCRs. Such a pioneering study has been reported recently where 49% of plasmon energy is estimated to be transferred to the dodecanethiol bonded with a 5 × 15-nm Au nanorod by direct charge transfer, almost two times larger than electron surface scattering (Figure 7D) (Foerster et al., 2017). Finally, significant advances in theoretically modeling are required to provide important insights into the elementary physicochemical steps as well as the dynamics of excited and ground molecular states in direct charge transfer process at length and timescale spanning from angstroms to hundreds of nanometers and femtoseconds to tens of picoseconds. For example, by exploiting time-dependent DFT, Norris et al. showed that the direct electron transfer probability in the interface of Ag-CO complex is largely dependent on the adsorption site of CO (Figure 7E) (Kumar et al., 2019). They further found that the charge density in real space shows coherent oscillations at 12 fs and loses coherence at 27 fs in response to the 10-fs laser pulse, suggesting that plasmon has decayed at 12 fs (Figure 7F). These observations provide a foundation for the development of plasmonic catalysts that support very high rates of the specific electronic excitations of adsorbates interacting with PMNs, thus efficiently enhancing particular chemical pathways.

PLASMON-INDUCED POTENTIALS

Under common chemical scenarios, the excited LSPs induce a potential at the surface of PMNs. Compared with the energetic charges and photothermal heating, it receives much less attention in the published studies on PMCRs. However, it has been recently demonstrated that plasmon-induced potentials modify the energetics and kinetics of a range of chemical reactions executed on illuminated PMNs (Wilson and Jain, 2020). There are multiple ways in which the potentials are generated on PMNs, such as optical rectification, the photothermoelectric effect, asymmetric charge transfer, and the plasmoelectric effect. Optical rectification is a phenomenon in which the interaction of highly intense light with nonlinear optical material generates a direct current polarization. Notably, the PMNs can rectify continuous wave due to the extreme enhancement of incident electric field at their surface, generating a potential (Ward et al., 2010). In thermoelectric effect, temperature gradient caused by the nonuniform photoheating of materials under illumination drives the carriers to flow across the gradient, resulting in a potential (Zolotavin et al., 2017). The photopotential induced by optical rectification and thermoelectric effect is small (~μV/mW). Their effects on PMCRs have been rarely reported either. We hereafter confine the discussion to the photopotential induced by asymmetric charge transfer and the photothermoelectric effect and its roles in PMCRs.

Energetic electrons and holes produced from the nonradiative decay of excited LSPs in PMNs would instantly recombine due to the absence of a band gap, or be transferred to charge acceptors in solution. Notably, they would not be removed at the same rate, i.e., asymmetric charge transfer, because of the different energy levels of electrons and holes as well as the distinct reactivity of their acceptors (Wilson and Jain, 2020). As a result, the energetic carrier of slower removal rate accumulates on PMNs and builds up a steady-state charge, giving rise to a photopotential. The magnitude of photopotentials was governed by the competing removal rate of electrons and holes. The photopotentials of Au and Ag sourced from asymmetric charge transfer were first reported by Brus' laboratory (Redmond and Brus, 2007; Redmond et al., 2007; Wu et al., 2010). They demonstrated that the potential of an indium tin oxide substrate coated with Ag NPs in the solution containing KNO_3 and sodium citrate was negatively shifted by ~140 mV under irradiation (shaded areas) with 488 nm light at an intensity of 100 mW/cm^3 (Figure 8A). This potential shift, namely, photopotential, was caused by the accumulation of energetic electrons produced from the excited Ag LSPs, whereas the energetic holes were rapidly scavenged by sodium citrates at their surface. When $AgNO_3$ were added, the measured potential shift was reduced to ~30 mV because the accumulated electrons were consumed by Ag^+. In other words, plasmon-induced potential drives the reduction of $AgNO_3$ at the surface of Ag NPs.

In plasmon-mediated ferricyanide reduction reaction on Au NPs, Jain et al. uncovered that the photopotential generated by asymmetric charge transfer reduces the reaction activation barrier and therefore accelerates the reaction rate (Figure 8B) (Kim et al., 2016). Under this scenario, holes occupied the d band of Au and were therefore highly reactive, whereas electrons distributed just above the Fermi level and were thus less chemically active. The holes were extracted readily from Au by transfer to a hole acceptor (e.g.,

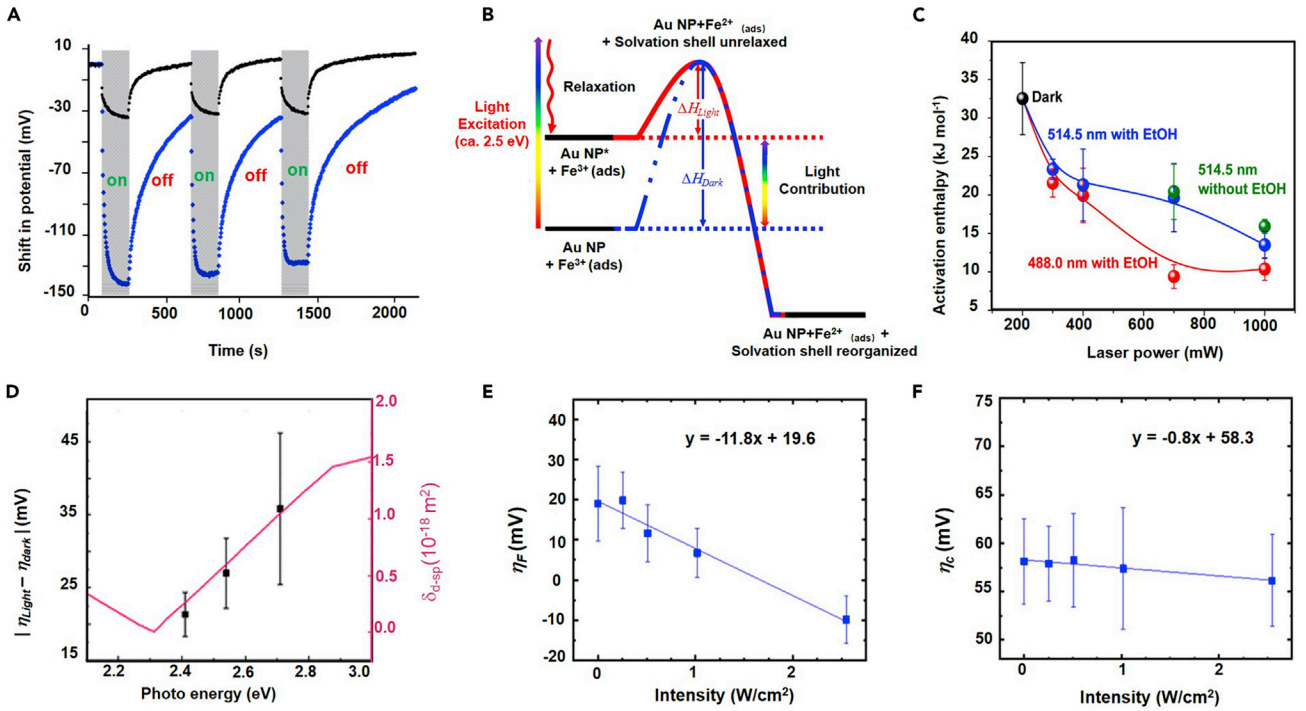

Figure 8. The photopotential sourced from asymmetric charge transfer and its impacts on chemical transformations on illuminated PMNs

(A) LSP-induced shift in the potential of an electrode composed of Ag NPs deposited on an indium tin oxide substrate in 0.1 M KNO_3 electrolyte with (black) or without (blue) Ag NO_3 (Redmond et al., 2007).

(B) Schematic of the reaction pathway and activation barrier (ΔH) for ferricyanide reduction reaction on Au NPs under light excitation and dark conditions (Kim et al., 2016).

(C) The dependence of activation enthalpy on the laser (488.0 and 514.5 nm) power with and without ethanol in (B). (D) The change in the onset overpotential of the hyrogen reduction reaction on Au NPs-coated glassy carbon electrode caused by light irradiation of different photonexcitation energies. The right y axis (pink) shows the photon-energy dependence of calculated interband absorption cross section of AuNPs (Wilson et al., 2019). The Faradaic, η_F, (E) and capacitive, η_C, (F) contribution to the onset potential of the hyrogen reduction reaction on illuminated Au NPs as a function of light intensity (Wilson et al., 2019).

H_2O), leading to a steady-state accumulation of electrons. These excess electrons raised the Fermi levels of Au up to ~240 meV under optimal conditions, which is equivalent to a cathodic potential of ~ −240 mV. As an outcome, the electrons at a cathodic potential from illuminated Au possessed a higher energy and overcame a lower energy barrier for ferricyanide reduction compared with that in dark. The magnitude of the reduction of apparent activation enthalpy was larger for photoexcitation at 488.0 nm (intraband transitions) than 514.5 nm (interband absorption) (Figure 8C). This was accounted for by the slower recombination rate of electron-hole pairs generated from interband transitions than intraband transitions, i.e., a larger fraction of electron-hole pairs survive the recombination process under 488.0 nm excitation, giving rise to a lager cathodic potential. The presence of ethanol in the reaction medium would enhance the scavenging rate of energetic holes, enlarge the catholic photopotential and therefore further lowering the activation enthalpy. Because the generation rate of electron-hole pair is proportional to the light intensity, the concentration of excess electrons is larger at higher intensities, generating a larger cathodic photopotential. Accordingly, the activation enthalpy was reduced when the laser power was increased (Figure 8C). In a recent publication, the impacts of light intensity on the photopotential and hence energetics of a reaction was even made quantitatively successfully (Yu and Jain, 2020).

The influence of photopotentials on reactivity extends to electrochemical reactions at PMNs under illumination (Wang et al., 2020; Huang et al., 2019). In electrochemical reactions, the onset overpotential (η) and current density signify the apparent activation barrier and total reaction rate, respectively. Jain et al. studied how excited LSPs affect the onset overpotential and current density of the electrochemical hydrogen evolution reaction (HER) on a film of Au NPs supported on a glassy carbon electrode in aqueous solution of 0.05 M H_2SO_4. They found that the onset overpotential under illumination (η_{light}) was remarkably

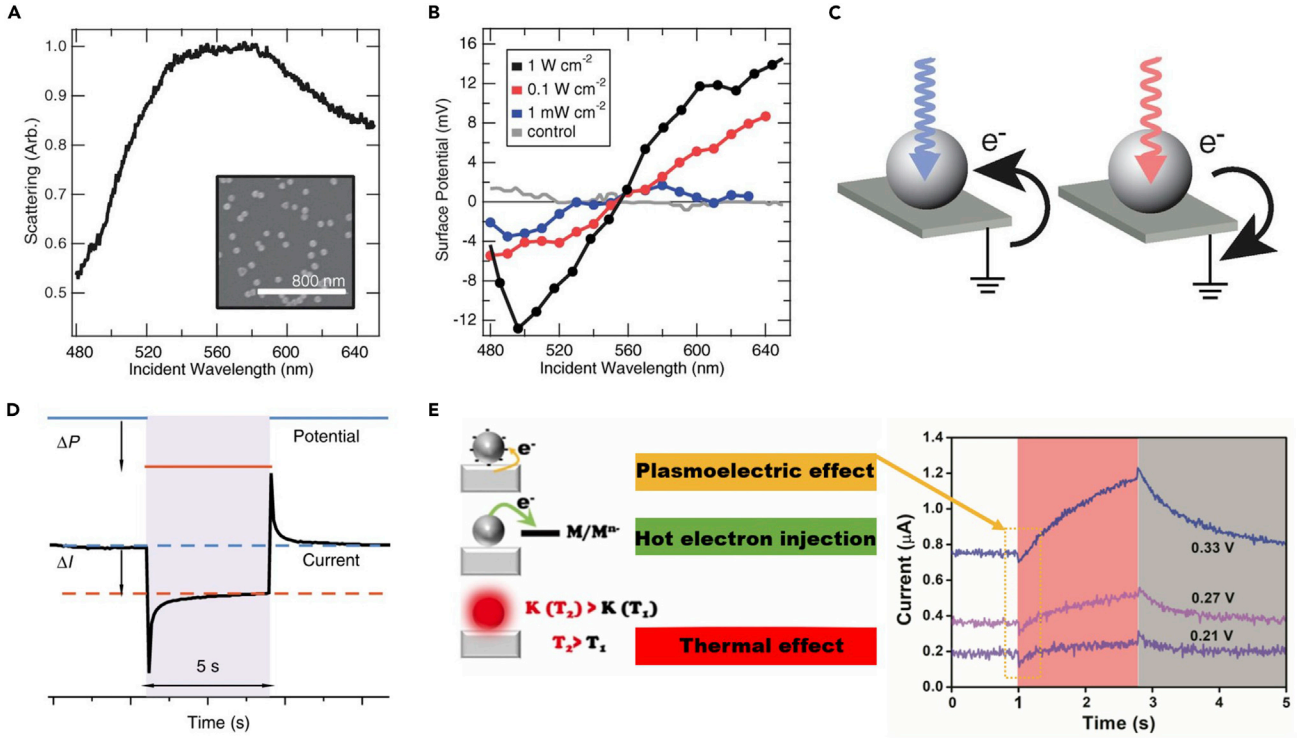

Figure 9. Plasmoelectric potential generation and their impacts in PMCRs

(A and B) (A) Dark-field scattering spectrum of 60-nm-diameter Au NPs (inset) on indium tin oxide/glass and (B) its surface potentials as a function of illumination wavelength for three different illumination intensities (Sheldon et al., 2014).

(C) Schematic of charge transfer to or from the NP under off-resonant excitation (Sheldon et al., 2014). Irradiation on the blue and red sides of the resonance leads to negative and positive charges, respectively (Sheldon et al., 2014).

(D) The typical chronoamperometry curve of plasmonic Au electrode in response to a potential step; ΔI is the current change induced by the step potential (ΔP) after a 5-s interval to stabilize (Zhan et al., 2019).

(E) Schematic illustrations of the three proposed plasmonic effects on nanostructured Ag electrode under illumination. Its photocurrents at 0.33 V, 0.27 V, and 0.21 V are given on the right with the response currents ascribed to plasmoelectric surface potentials in the yellow dotted circle (Ou et al., 2020).

deviated from that in dark conditions (η_{dark}), supporting that the apparent activation barrier of reaction was decreased by light excitation (Figure 8D). It is reasonable that the illuminated NPs supply electrons at a more negative potential due to photopotential, lowering the energy barrier of charge transfer in the reaction. The magnitude of decrease in activation barrier, $|\eta_{light} - \eta_{dark}|$, was expanded when excitation wavelength was blue-shifted, which is consistent with the wavelength dependence of the calculated interband absorption cross section. It was further demonstrated that the Faradaic contribution to the onset overpotential, η_F, decreased ~30 mV when light intensity was increased from 0 to 2.55 W/cm^2 (Figure 8E). In contrast, the capacitive contribution to the onset overpotential, η_c, changed by a marginal amount (~2 mV) with the same range (Figure 8F). These results suggested that the photopotential exclusively modulates the Faradaic reaction, fundamentally different from an applied DC potential that drives both the Faradaic reaction and capacitive charging process. Moreover, asymmetric charge transfer can be modulated by the applied electrode voltage in addition to light intensity, excitation wavelength, and charge scavenges, providing another means for controlling the photopotential. For example, under a larger negative bias, energetic holes would be much more rapidly removed into the external circuit, resulting in a bigger cathodic potential on the Au NPs. To sum up, the potential sourced from asymmetric charge transfer provides an effective means for manipulating the energetics and kinetics of both chemical and electrochemical reactions.

In 2014, Atwater et al. put forth "plasmoelectric potentials" in their pioneering study on the surface electric field of PMNs that were illuminated with monochromatic light under the off-resonant conditions (Figures 9A–9C) (Sheldon et al., 2014). They detected negative and positive surface potentials at both Au NP arrays and Au nanohole arrays under the impingement of light with energy above or below the plasmon

resonance, respectively. A theoretical explanation was proposed: the thermal fluctuations induced the electron transfer to/from their underlying substrate, enabling the wavelength of LSPR approach that of excited light; this enhanced the optical absorption of Au NP, further raising their temperature; the temperature increase caused additional charge transfer in the same direction, generating the observed surface potentials. Such a plasmoelectric effect is essentially driven by the entropy increase that occurs when the off-resonantly excited PMNs align their plasmon-resonant frequency with the incident light wavelength by varying their charge density for lowering the total free energy (Van De Groep et al., 2016). Zhao et al. exploited Kelvin probe force microscopy to map plasmoelectric potentials on single Au and Ag NPs, unveiling height-related surface potential information and the charge density evolution process (Zhao et al., 2018). The results showed that Au and Ag NP have opposite plasmoelectric potentials under the same excitation source due to their distinct LSP frequencies. The plasmoelectric potential is quantified based on a statistical method, which reaches −79 and 54 mV on Au NP and Ag NP under light illumination at the intensity of 5.4 mW/cm^2, respectively. It was demonstrated that merely measuring of the UV-visible spectrum of Au NPs is sufficient to alter their charge densities and hence induce plasmoelectric potentials (Navarrete et al., 2018).

Plasmoelectric potentials are expected to affect the reaction outcomes at the surface of PMNs in multiple ways. If the reaction is photocatalytic reaction, the positive surface plasmoelectric potential would enhance the interaction between negative absorbates and reactive sites and weaken the binding capacity of positive absorbates with PMNs due to Coulombic forces. The opposite situation would occur when the negative surface plasmoelectric potential was generated. In other words, the adsorption/desorption behaviors of charged reactants, intermediates, and products will be modified, possibly leading to distinct reaction outcomes. In the case of electrocatalytic reaction, apart from mediating the adsorption/desorption behaviors of active species, this plasmoelectric potential will accelerate electrochemical transformations by changing effective overpotential, or contribute to the apparent currents by capacitively charging. For example, Ren et al. showed that the rapid response current of the Au nanoelectrode array under illumination can be reproduced by the Au nanoelectrode under a pulsed potential. Based on that, they concluded that the plasmoelectric potential enhanced the electrochemical reaction and led to a rapid response current (Figure 9D) (Zhan et al., 2019). Furthermore, it was found the increment of current was more remarkable at larger applied biases, suggesting that the applied potential can promote the formation of plasmoelectric potential. In our previous study on the plasmon-mediated electrochemistry at nanostructured Ag electrodes, we found that the plasmoelectric effects led to a capacitive current (~60 nA), which bore the opposite sign of dark current at the anodic biases, contributing to the nonthermal effects (Figure 9E) (Ou et al., 2020). To date, the exploiting of plasmoelectric potentials in PMCRs is still in its infancy. Future work in this area will benefit from further investigation into the microscopic mechanisms that contribute to the observed effects and that modulate the chemical transformations at PMNs.

CONCLUSION

PMNs provide a wealth of opportunities for manipulating PMCRs, thanks to the desirable optical properties originating from their LSPs. Although the improved selectivity and efficiency in PMCRs has been clearly demonstrated in literatures, further fundamental and application studies are needed to unleash their full potentials. Perspectives are offered for uncovering the specific physicochemical mechanisms predominantly responsible for the enhanced reaction rate and the improved product yield and selectivity in PMCRs. A reliable method to quantify thermal and nonthermal contributions in PMCRs would be a must for determining whether the reaction is predominantly driven by plasmon-induced carriers or heat. For carrier-driven reactions, it is important to find out whether the carriers are transported to adsorbates at the instant of LSPs' dephasing (direct), or after the dephasing (indirect), which would lead to different optical energy utilization efficiency and controllability of product distribution. Apart from energetic charge carriers, plasmon-induced potentials are expected to make a significant contribution to the nonthermal effects, which deserve more research attention.

ACKNOWLEDGMENTS

J.L. gratefully acknowledges that the work was jointly supported by the National Key R&D Program of China (Project No. 2017YFA0204403), the Innovation and Technology Commission of HKSAR through Hong Kong Branch of National Precious Metals Material Engineering Research Centre, and the Centre for Functional

Photonics at City University of Hong Kong. W. O. thanks Prof. Jiang Jiang from Suzhou Institute of Nano-Tech and Nano-Bionics (SINANO), Chinese Academy of Sciences, for his helpful comments.

AUTHOR CONTRIBUTIONS

J.L. conceptualized and supervised the work. W.O. wrote the manuscript. Y.Y.L. revised the manuscript. B.Z. drew Figures 2, 3, 4, 5, 6, 7, 8, and 9; participated in discussion; and checked the manuscript. J.S. drew Figure 1 and contributed to the physical interpretation of plasmon. C.Z. checked the manuscript and participated in discussion.

REFERENCES

Andoy, N.M., Zhou, X., Choudhary, E., Shen, H., Liu, G., and Chen, P. (2013). Single-molecule catalysis mapping quantifies site-specific activity and uncovers radial activity gradient on single 2d nanocrystals. J. Am. Chem. Soc. *135*, 1845–1852.

Atwater, H.A., and Polman, A. (2010). Plasmonics for improved photovoltaic devices. Nat. Mater. *9*, 205–213.

Baffou, G., Girard, C., and Quidant, R. (2010a). Mapping heat origin in plasmonic structures. Phys. Rev. Lett. *104*, 136805.

Baffou, G., Quidant, R., and García De Abajo, F.J. (2010b). Nanoscale control of optical heating in complex plasmonic systems. ACS Nano *4*, 709–716.

Baffou, G., Berto, P., Bermudez, U.E., Quidant, R., Monneret, S., Polleux, J., and Rigneault, H. (2013). Photoinduced heating of nanoparticle arrays. ACS Nano *7*, 6478–6488.

Baffou, G., Bordacchini, I., Baldi, A., and Quidant, R. (2020). Simple experimental procedures to distinguish photothermal from hot-carrier processes in plasmonics. Light Sci. Appl. *9*, 108–124.

Barella, M., Violi, I.L., Gargiulo, J., Martinez, L.P., Goschin, F., Guglielmotti, V., Pallarola, D., Schlucker, S., Pilo-Pais, M., Acuna, G.P., et al. (2020). In situ photothermal response of single gold nanoparticles through hyperspectral imaging anti-stokes thermometry. ACS Nano. https://doi.org/10.1021/acsnano.0c06185.

Block, A., Liebel, M., Yu, R., Spector, M., Abajo, J.G., Sivan, Y., and Hulst, N.F. (2019). Tracking ultrafast hot-electron diffusion in space and time by ultrafast thermomodulation microscopy. Sci. Adv. *5*, eaav8965.

Boyer, D., Tamarat, P., Maali, A., Lounis, B., and Orrit, M. (2002). Photothermal imaging of nanometer-sized metal particles among scatterers. Science *297*, 1160.

Brongersma, M.L., Halas, N.J., and Nordlander, P. (2015). Plasmon-induced hot carrier science and technology. Nat. Nanotechnol. *10*, 25–34.

Boerigter, C., Aslam, U., and Linic, S. (2016). Mechanism of charge transfer from plasmonic nanostructures to chemically attached materials. ACS Nano *10*, 6108–6115.

Brown, A.M., Sundararaman, R., Narang, P., Goddard, W.A., and Atwater, H.A. (2016). ACS Nano *10*, 957–966.

Chen, T., Zhang, Y., and Xu, W. (2016). Single-molecule nanocatalysis reveals catalytic activation energy of single nanocatalysts. J. Am. Chem. Soc. *138*, 12414–12421.

Christopher, P., Xin, H., and Linic, S. (2011). Visible-light-enhanced catalytic oxidation reactions on plasmonic silver nanostructures. Nat. Chem. *3*, 467–472.

Christopher, P., Xin, H., Marimuthu, A., and Linic, S. (2012). Singular characteristics and unique chemical bond activation mechanisms of photocatalytic reactions on plasmonic nanostructures. Nat. Mater. *11*, 1044–1050.

Corson, E.R., Creel, E.B., Kostecki, R., Mccloskey, B.D., and Urban, J.J. (2020). Important considerations in plasmon-enhanced electrochemical conversion at voltage-biased electrodes. iScience *23*, 100911.

Cortes, E., Xie, W., Cambiasso, J., Jermyn, A.S., Sundararaman, R., Narang, P., Schlucker, S., and Maier, S.A. (2017). Plasmonic hot electron transport drives nano-localized chemistry. Nat. Commun. *8*, 14880.

Ding, X., Liow, C.H., Zhang, M., Huang, R., Li, C., Shen, H., Liu, M., Zou, Y., Gao, N., Zhang, Z., et al. (2014). Surface plasmon resonance enhanced light absorption and photothermal therapy in the second near-infrared window. J. Am. Chem. Soc. *136*, 15684–15693.

Dubi, Y., Un, I.W., and Sivan, Y. (2020). Thermal effects – an alternative mechanism for plasmon-assisted photocatalysis. Chem. Sci. *11*, 5017–5027.

Engelbrekt, C., Crampton, K.T., Fishman, D.A., Law, M., and Apkarian, V.A. (2020). Efficient plasmon-mediated energy funneling to the surface of Au@pt core-shell nanocrystals. ACS Nano *14*, 5061–5074.

Fasciani, C., Alejo, C.J.B., Grenier, M., Netto-Ferreira, J.C., and Scaiano, J.C. (2011). High-temperature organic reactions at room temperature using plasmon excitation: decomposition of dicumyl peroxide. Org. Lett. *13*, 204–207.

Foerster, B., Joplin, A., Kaefer, K., Celiksoy, S., Link, S., and Sonnichsen, C. (2017). Chemical interface damping depends on electrons reaching the surface. ACS Nano *11*, 2886–2893.

Huang, L., Zou, J., Ye, J.Y., Zhou, Z.Y., Lin, Z., Kang, X., Jain, P.K., and Chen, S. (2019). Synergy between plasmonic and electrocatalytic activation of methanol oxidation on palladium-silver alloy nanotubes. Angew. Chem. Int. Ed. *58*, 8794–8798.

Jain, P. K. (2020). Comment on "thermal effects – an alternative mechanism for plasmon-assisted photocatalysis" by Y. Dubi, I. W. Un and Y. Sivan, Chem. Sci., 2020, 11, 5017

Jiang, R., Li, B., Fang, C., and Wang, J. (2014). Metal/semiconductor hybrid nanostructures for plasmon-enhanced applications. Adv. Mater. *26*, 5274–5309.

Kale, M.J., Avanesian, T., and Christopher, P. (2013). Direct photocatalysis by plasmonic nanostructures. ACS Catal. *4*, 116–128.

Kim, Y., Dumett Torres, D., and Jain, P.K. (2016). Activation energies of plasmonic catalysts. Nano Lett. *16*, 3399–3407.

Knight, M.W., Sobhani, H., Nordlander, P., and Halas, N.J. (2011). Photodetection with active optical antennas. Science *332*, 702–704.

Kumar, P.V., Rossi, T.P., Kuisma, M., Erhart, P., and Norris, D.J. (2019). Direct hot-carrier transfer in plasmonic catalysis. Faraday Discuss. *214*, 189–197.

Lee, S.Y., Tsalu, P.V., Kim, G.W., Seo, M.J., Hong, J.W., and Ha, J.W. (2019). Tuning chemical interface damping: interfacial electronic effects of adsorbate molecules and sharp tips of single gold bipyramids. Nano Lett. *19*, 2568–2574.

Linic, S., Christopher, P., and Ingram, D.B. (2011). Plasmonic-metal nanostructures for efficient conversion of solar to chemical energy. Nat. Mater. *10*, 911–921.

Linic, S., Aslam, U., Boerigter, C., and Morabito, M. (2015). Photochemical transformations on plasmonic metal nanoparticles. Nat. Mater. *14*, 567–576.

Li, X., Xiao, D., and Zhang, Z. (2013). Landau damping of quantum plasmons in metal nanostructures. New J. Phys. *15*, 023011.

Li, S., Miao, P., Zhang, Y., Wu, J., Zhang, B., Du, Y., Han, X., Sun, J., and Xu, P. (2020a). Recent advances in plasmonic nanostructures for enhanced photocatalysis and electrocatalysis. Adv. Mater. e2000086.

Li, W., Miao, J., Peng, T., Lv, H., Wang, J.G., Li, K., Zhu, Y., and Li, D. (2020b). Single-molecular catalysis identifying activation energy of the intermediate product and rate-limiting step in plasmonic photocatalysis. Nano Lett. *20*, 2507–2513.

Liu, N., Tang, M.L., Hentschel, M., Giessen, H., and Alivisatos, A.P. (2011). Nanoantenna-enhanced gas sensing in a single tailored nanofocus. Nat. Mater. *10*, 631–636.

Maley, M., Hill, J.W., Saha, P., Walmsley, J.D., and Hill, C.M. (2019). The role of heating in the electrochemical response of plasmonic nanostructures under illumination. J. Chem. Phys. C *123*, 12390–12399.

Marimuthu, A., Zhang, J., and Linic, S. (2013). Tuning selectivity in propylene epoxidation by plasmon mediated photo-switching of cu oxidation state. Science *339*, 1590–1593.

Miliutina, E., Guselnikova, O., Soldatova, N.S., Bainova, P., Elashnikov, R., Fitl, P., Kurten, T., Yusubov, M.S., Svorcik, V., Valiev, R.R., et al. (2020). Can plasmon change reaction path? Decomposition of unsymmetrical iodonium salts as an organic probe. J. Phys. Chem. Lett. *11*, 5770–5776.

Ming, T., Chen, H., Jiang, R., Li, Q., and Wang, J. (2012). Plasmon-controlled fluorescence: beyond the intensity enhancement. J. Phys. Chem. Lett. *3*, 191–202.

Mubeen, S., Lee, J., Singh, N., Kramer, S., Stucky, G.D., and Moskovits, M. (2013). An autonomous photosynthetic device in which all charge carriers derive from surface plasmons. Nat. Nanotechnol. *8*, 247–251.

Mukherjee, S., Libisch, F., Large, N., Neumann, O., Brown, L.V., Cheng, J., Lassiter, J.B., Carter, E.A., Nordlander, P., and Halas, N.J. (2013). Hot electrons do the impossible: plasmon-induced dissociation of H_2 on Au. Nano Lett. *13*, 240–247.

Mukherjee, S., Zhou, L., Goodman, A.M., Large, N., Ayala-Orozco, C., Zhang, Y., Nordlander, P., and Halas, N.J. (2014). Hot-electron-induced dissociation of H_2 on gold nanoparticles supported on SiO_2. J. Am. Chem. Soc. *136*, 64–67.

Navarrete, J., Siefe, C., Alcantar, S., Belt, M., Stucky, G.D., and Moskovits, M. (2018). Merely measuring the UV–visible spectrum of gold nanoparticles can change their charge state. Nano Lett. *18*, 669–674.

Ou, W., Zhou, B., Shen, J., Lo, T.W., Lei, D., Li, S., Zhong, J., Li, Y.Y., and Lu, J. (2020). Thermal and nonthermal effects in plasmon-mediated electrochemistry at nanostructured ag electrodes. Angew. Chem. Int. Ed. *59*, 6790–6793.

Rao, V.G., Aslam, U., and Linic, S. (2019). Chemical requirement for extracting energetic charge carriers from plasmonic metal nanoparticles to perform electron-transfer reactions. J. Am. Chem. Soc. *141*, 643–647.

Reddy, H., Wang, K., Kudyshev, Z., Zhu, L., Yan, S., Vezzoli, A., Higgins, S.J., Gavini, V., Boltasseva, A., Reddy, P., et al. (2020). Determining plasmonic hot-carrier energy distributions via single-molecule transport measurements. Science *369*, 423–426.

Redmond, P.L., and Brus, L.E. (2007). "Hot electron" photo-charging and electrochemical discharge kinetics of silver nanocrystals. J. Chem. Phys. C *111*, 14849–14854.

Redmond, P.L., Wu, X., and Brus, L. (2007). Photovoltage and photocatalyzed growth in citrate-stabilized colloidal silver nanocrystals. J. Chem. Phys. C *111*, 8942–8947.

Richard-Lacroix, M., and Deckert, V. (2020). Direct molecular-level near-field plasmon and temperature assessment in a single plasmonic hotspot. Light Sci. Appl. *9*, 35.

Richardson, H.H., Carlson, M.T., Tandler, P.J., Hernandez, P., and Govorov, A.O. (2009). Experimental and theoretical studies of light-to-heat conversion and collective heating effects in metal nanoparticle solutions. Nano Lett. *9*, 1139–1146.

Robatjazi, H., Zhao, H., Swearer, D.F., Hogan, N.J., Zhou, L., Alabastri, A., Mcclain, M.J., Nordlander, P., and Halas, N.J. (2017). Plasmon-induced selective carbon dioxide conversion on earth-abundant aluminum-cuprous oxide antenna-reactor nanoparticles. Nat. Commun. *8*, 27.

Rodio, M., Graf, M., Schulz, F., Mueller, N.S., Eich, M., and Lange, H. (2020). Experimental evidence for nonthermal contributions to plasmon-enhanced electrochemical oxidation reactions. ACS Catal. *10*, 2345–2353.

Schorr, N.B., Counihan, M.J., Bhargava, R., and Rodriguez-Lopez, J. (2020). Impact of plasmonic photothermal effects on the reactivity of Au nanoparticle modified graphene electrodes visualized using scanning electrochemical microscopy. Anal. Chem *92*, 3666–3673.

Sheldon, M.T., Van De Groep, J., Brown, A.M., Polman, A., and Atwater, H.A. (2014). Plasmoelectric potentials in metal nanostructures. Science *346*, 828–830.

Simoncelli, S., Li, Y., Cortes, E., and Maier, S.A. (2018). Nanoscale control of molecular self-assembly induced by plasmonic hot-electron dynamics. ACS Nano *12*, 2184–2192.

Simoncelli, S., Pensa, E.L., Brick, T., Gargiulo, J., Lauri, A., Cambiasso, J., Li, Y., Maier, S.A., and Cortes, E. (2019). Monitoring plasmonic hot-carrier chemical reactions at the single particle level. Faraday Discuss. *214*, 73–87.

Sivan, Y., and Spector, M. (2020). Ultrafast dynamics of optically induced heat gratings in metals. ACS Photon. *7*, 1271–1279.

Sivan, Y., Baraban, J., Un, I.W., and Dubi, Y. (2019a). Comment on "quantifying hot carrier and thermal contributions in plasmonic photocatalysis". Science *364*, eaaw9367.

Sivan, Y., Un, I.W., and Dubi, Y. (2019b). Assistance of metal nanoparticles in photocatalysis - nothing more than a classical heat source. Faraday Discuss. *214*, 215–233.

Sivan, Y., Baraban, J.H., and Dubi, Y. (2020). Experimental practices required to isolate thermal effects in plasmonic photo-catalysis: lessons from recent experiments. OSA Continuum *3*, 483–497.

Sun, C.K., Vallée, F., Acioli, L.H., Ippen, E.P., and Fujimoto, J.G. (1994). Femtosecond-tunable measurement of electron thermalization in gold. Phys. Rev. B *50*, 15337–15348.

Tachikawa, T., Yonezawa, T., and Majima, T. (2013). Super-resolution mapping of reactive sites on titania-based nanoparticles with water-soluble fluorogenic probes. ACS Nano *7*, 263–275.

Therrien, A.J., Kale, M.J., Yuan, L., Zhang, C., Halas, N.J., and Christopher, P. (2019). Impact of chemical interface damping on surface plasmon dephasing. Faraday Discuss. *214*, 59–72.

Ueno, K., Juodkazis, S., Shibuya, T., Yokota, Y., Mizeikis, V., Sasaki, K., and Misawa, H. (2008). Nanoparticle plasmon-assisted two-photon polymerization induced by incoherent excitation source. J. Am. Chem. Soc. *130*, 6928–6929.

Un, I.W., and Sivan, Y. (2020). Parametric study of temperature distribution in plasmon-assisted photocatalysis. Nanoscale *12*, 17821–17832.

Vadai, M., Angell, D.K., Hayee, F., Sytwu, K., and Dionne, J.A. (2018). In-situ observation of plasmon-controlled photocatalytic dehydrogenation of individual palladium nanoparticles. Nat. Commun. *9*, 4658.

Van De Groep, J., Sheldon, M.T., Atwater, H.A., and Polman, A. (2016). Thermodynamic theory of the plasmoelectric effect. Sci. Rep. *6*, 23283.

Wang, J., Heo, J., Chen, C., Wilson, A.J., and Jain, P.K. (2020). Ammonia oxidation enhanced by photopotential generated by plasmonic excitation of a bimetallic electrocatalyst. Angew. Chem. Int. Ed. *59*, 18430–18434.

Ward, D.R., Hüser, F., Pauly, F., Cuevas, J.C., and Natelson, D. (2010). Optical rectification and field enhancement in a plasmonic nanogap. Nat. Nanotechnol. *5*, 732–736.

Willets, K.A., and Van Duyne, R.P. (2007). Localized surface plasmon resonance spectroscopy and sensing. Annu. Rev. Phys. Chem. *58*, 267–297.

Wilson, A.J., and Jain, P.K. (2020). Light-induced voltages in catalysis by plasmonic nanostructures. Acc. Chem. Res. *53*, 1773–1781.

Wilson, A.J., Mohan, V., and Jain, P.K. (2019). Mechanistic understanding of plasmon-enhanced electrochemistry. J. Chem. Phys. C *123*, 29360–29369.

Wu, X., Thrall, E.S., Liu, H., Steigerwald, M., and Brus, L. (2010). Plasmon induced photovoltage and charge separation in citrate-stabilized gold nanoparticles. J. Chem. Phys. C *114*, 12896–12899.

Yan, J., Jacobsen, K.W., and Thygesen, K.S. (2011). First-principles study of surface plasmons on Ag(111) and H/Ag(111). Phys. Rev. B *84*, 235430.

Yu, S., and Jain, P.K. (2020). The chemical potential of plasmonic excitations. Angew. Chem. Int. Ed. *59*, 2085–2088.

Yu, Y., Sundaresan, V., and Willets, K.A. (2018a). Hot carriers versus thermal effects: resolving the enhancement mechanisms for plasmon-mediated photoelectrochemical reactions. J. Chem. Phys. C *122*, 5040–5048.

Yu, Y., Williams, J.D., and Willets, K.A. (2018b). Quantifying photothermal heating at plasmonic nanoparticles by scanning electrochemical microscopy. Faraday Discuss. *210*, 29–39.

Zhan, C., Chen, X.-J., Yi, J., Li, J.-F., Wu, D.-Y., and Tian, Z.-Q. (2018). From plasmon-enhanced molecular spectroscopy to plasmon-mediated chemical reactions. Nat. Rev. Chem. *2*, 216–230.

Zhan, C., Liu, B.-W., Huang, Y.-F., Hu, S., Ren, B., Moskovits, M., and Tian, Z.-Q. (2019). Disentangling charge carrier from photothermal effects in plasmonic metal nanostructures. Nat. Commun. *10*, 2671.

Zhang, X., Li, X., Zhang, D., Su, N.Q., Yang, W., Everitt, H.O., and Liu, J. (2017). Product selectivity in plasmonic photocatalysis for carbon dioxide hydrogenation. Nat. Commun. *8*, 14542.

Zhang, Y., He, S., Guo, W., Hu, Y., Huang, J., Mulcahy, J.R., and Wei, W.D. (2018a). Surface-plasmon-driven hot electron photochemistry. Chem. Rev. *118*, 2927–2954.

Zhang, X., Li, X., Reish, M.E., Zhang, D., Su, N.Q., Gutiérrez, Y., Moreno, F., Yang, W., Everitt, H.O., and Liu, J. (2018b). Plasmon-enhanced catalysis: distinguishing thermal and nonthermal effects. Nano Lett. *18*, 1714–1723.

Zhao, M., and Chen, P. (2020). Exploring plasmonic photocatalysis via single-molecule reaction imaging. Nano Lett. *20*, 2939–2940.

Zhao, F., Yang, W., Shih, T.-M., Feng, S., Zhang, Y., Li, J., Yan, J., and Yang, Z. (2018). Plasmoelectric potential mapping of a single nanoparticle. ACS Photon. *5*, 3519–3525.

Zhou, X., Andoy, N.M., Liu, G., Choudhary, E., Han, K.S., Shen, H., and Chen, P. (2012). Quantitative super-resolution imaging uncovers reactivity patterns on single nanocatalysts. Nat. Nanotechnol. *7*, 237–241.

Zhou, L., Swearer, D.F., Zhang, C., Robatjazi, H., Zhao, H., Henderson, L., Dong, L., Christopher, P., Carter, E.A., Nordlander, P., and Halas, N.J. (2018). Quantifying hot carrier and thermal contributions in plasmonic photocatalysis. Science *362*, 69–72.

Zhou, L., Swearer, D.F., Robatjazi, H., Alabastri, A., Christopher, P., Carter, E.A., Nordlander, P., and Halas, N.J. (2019). Response to comment on "quantifying hot carrier and thermal contributions in plasmonic photocatalysis". Science *364*, eaaw9545.

Zijlstra, P., Paulo, P.M., Yu, K., Xu, Q.H., and Orrit, M. (2012). Chemical interface damping in single gold nanorods and its near elimination by tip-specific functionalization. Angew. Chem. Int. Ed. *51*, 8352–8355.

Zolotavin, P., Evans, C., and Natelson, D. (2017). Photothermoelectric effects and large photovoltages in plasmonic au nanowires with nanogaps. J. Phys. Chem. Lett. *8*, 1739–1744.

Zou, N., Chen, G., Mao, X., Shen, H., Choudhary, E., Zhou, X., and Chen, P. (2018). Imaging catalytic hotspots on single plasmonic nanostructures via correlated super-resolution and electron microscopy. ACS Nano *12*, 5570–5579.